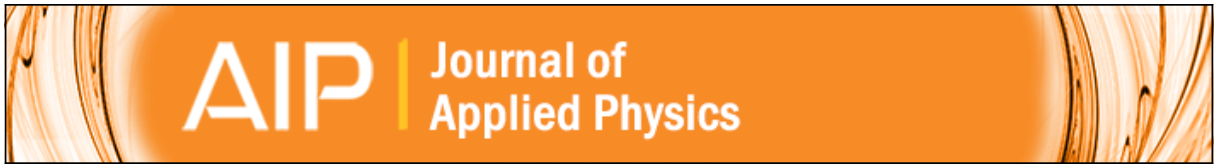

Experimental and theoretical investigation of the structural, chemical, electronic, and high frequency dielectric properties of barium cadmium tantalate–based ceramics

Shaojun Liu, Richard Taylor, Novak S. Petrovic, Louisa Budd, Mark Van Schilfgaarde, and N. Newman

Citation: Journal of Applied Physics **97**, 014105 (2005); doi: 10.1063/1.1823575

View online: http://dx.doi.org/10.1063/1.1823575

View Table of Contents: http://scitation.aip.org/content/aip/journal/jap/97/1?ver=pdfcov

Published by the AIP Publishing

Experimental and theoretical investigation of the structural, chemical, electronic, and high frequency dielectric properties of barium cadmium tantalate–based ceramics

Shaojun Liu
Chemical and Materials Engineering Department, Arizona State University, Tempe, Arizona 85287-6006

Richard Taylor and Novak S. Petrovic
School of Information and Electrical Engineering, University of Queensland, St. Lucia Queensland 4064, Brisbane, Australia

Louisa Budd, Mark Van Schilfgaarde, and N. Newman[a)]
Science and Engineering of Materials Program and Chemical and Materials Engineering Department, Arizona State University, Tempe, Arizona 85287-6006

(Received 15 July 2004; accepted 29 September 2004; published online 14 December 2004)

Single-phase $Ba(Cd_{1/3}Ta_{2/3})O_3$ powder was produced using conventional solid state reaction methods. $Ba(Cd_{1/3}Ta_{2/3})O_3$ ceramics with 2 wt % ZnO as sintering additive sintered at 1550 °C exhibited a dielectric constant of ~32 and loss tangent of 5×10^{-5} at 2 GHz. X-ray diffraction and thermogravimetric measurements were used to characterize the structural and thermodynamic properties of the material. *Ab initio* electronic structure calculations were used to give insight into the unusual properties of $Ba(Cd_{1/3}Ta_{2/3})O_3$, as well as a similar and more widely used material $Ba(Zn_{1/3}Ta_{2/3})O_3$. While both compounds have a hexagonal Bravais lattice, the P321 space group of $Ba(Cd_{1/3}Ta_{2/3})O_3$ is reduced from $P\bar{3}m1$ of $Ba(Zn_{1/3}Ta_{2/3})O_3$ as a result of a distortion of oxygen away from the symmetric position between the Ta and Cd ions. Both of the compounds have a conduction band minimum and valence band maximum composed of mostly weakly itinerant Ta 5*d* and Zn 3*d*/Cd 4*d* levels, respectively. The covalent nature of the directional *d*-electron bonding in these high-*Z* oxides plays an important role in producing a more rigid lattice with higher melting points and enhanced phonon energies, and is suggested to play an important role in producing materials with a high dielectric constant and low microwave loss. © *2005 American Institute of Physics*. [DOI: 10.1063/1.1823575]

I. INTRODUCTION

Miniaturization of satellite communication and cellular systems requires low-loss temperature-compensated microwave ceramics with enhanced dielectric constants.[1,2] Since 1970s, there have been significant advances in the performance of several microwave dielectric ceramics, including $Ba_2Ti_9O_{20}$, $BaTi_4O_9$, $Zr_{1-x}Sn_xTiO_4$, $Ba(Zn_{1/3}Ta_{2/3})O_3$, and $Ba_{6-3x}RE_{8+2x}Ti_{18}O_{54}$ (RE—rare earth).[3] The performance of dielectric filters has significantly improved as a result of these advances, as well as from improvements in device and system design.[4]

$Ba(B_{1/3}Ta_{2/3})O_3$ based perovskite compounds, where *B* = Mg and Zn show tremendous potential for widespread use in microwave systems owing to their excellent high frequency properties. $Ba(Zn_{1/3}Ta_{2/3})O_3$, for example, has a large dielectric constant ($\varepsilon\sim30$) and ultra-low-loss tangent ($\tan\delta<2\times10^{-5}$ at 2 GHz). Furthermore, when doped with Ni, its temperature coefficient of resonant frequency τ_f can be tuned to near zero.[5] Zr is also commonly added since it has been found that high quality factors *Q* can be obtained in much shorter annealing times.[6]

As yet we do not have a fundamental understanding of why this class of materials can have both a high dielectric constant and low loss, although a number of experimental and theoretical investigations have proposed that the permittivity is entirely dominated by polar phonon mode contributions described by a classical oscillator mode[7] and the predominant microwave loss mechanism in practical dielectric arises from the low-energy tail of anharmonic lattice vibrations.[7–9]

A basic understanding of the mechanisms of microwave loss in practical materials has eluded researchers to date, but a number of material properties have shown to be strongly correlated with loss. For example, an early paper reported an inverse relationship between Zn–Ta site ordering in $Ba(Zn_{1/3}Ta_{2/3})O_3$ (typically referred to as *B*-site ordering in $A(B_{1/3}B'_{2/3})O_3$ perovskites) and the loss tangent at microwave frequencies.[10] It was reported that high-quality factors and *B*-site ordering could be attained through high temperature annealing at 1350 °C for extended periods (120 h). Microwave loss in other materials, including $ZrTiO_4$ doping with Sn, has also been correlated with cation ordering.[11] Later reports found that the addition of $BaZrO_3$ to $Ba(Zn_{1/3}Ta_{2/3})O_3$ resulted in low loss even without extended annealing times and significant *B*-site ordering.[6] A number of reports attributed this to various factors, including specific atomic configurations at grain boundaries.[12] The amount of impurities in the material has also been correlated to the

[a)]Author to whom correspondence should be addressed; electronic mail: nate.newman@asu.edu

microwave loss.[13] A recent report found a direct correlation between microwave loss and the concentration of point defects, as quantified by optical spectroscopy.[2] Clearly the role of intrinsic and extrinsic factors in the microwave loss process in these materials is just beginning to be uncovered.

In this paper, we report an experimental and theoretical investigation aimed at understanding the chemical and physical properties of high performance microwave dielectrics. We chose to study $Ba(Cd_{1/3}Ta_{2/3})O_3$ based materials since initial theoretical calculations predict that the relative contribution of *d*-electron bonding will be stronger in Cd-containing compounds than in other $A(B_{1/3}Ta_{2/3})O_3$ perovskites. Prior work that measured low frequency properties of $Ba(Zn_xCd_{1/3-x}Ta_{2/3})O_3$ alloys reported a maximum dielectric constant of ~30 at 1 kHz.[14]

II. EXPERIMENTAL PROCEDURES AND THEORETICAL APPROACH

$Ba(Cd_{1/3}Ta_{2/3})O_3$ powder was made from reagent grade $BaCO_3$, Ta_2O_3, and CdO. The raw powders were blended using distilled water and ZrO_2 ball milling media (diameter ~1 cm) with a 20:1 milling ball to powder weight ratio for 16 h in a milling machine. This step served to deagglomerate the powders and provide a homogeneous distribution of raw powders. The slurry was subsequently dried. The dried powder was filtered through a 14-mesh screen. Then, the powder was heated to 1350 °C for 10 h with an initial ramp of 100 °C/h in air in a box furnace (CM furnaces Model 1700) to bring about reaction of the raw powder to form single-phase powder. After the reaction step, the $Ba(Cd_{1/3}Ta_{2/3})O_3$ powder was milled in a poly(vinylacohol)-poly(ethylene glycol) aqueous slurry in order to reduce the particle size to that which will facilitate densification during sintering. $Ba(Cd_{1/3-x}Zn_xTa_{2/3})O_3$ alloy powders were also produced with the same procedure using reagent grade $BaCO_3$, Ta_2O_3, ZnO, and CdO. To produce the $Ba(Cd_{1/3}Ta_{2/3})O_3$ compound, the addition of 2 wt % ZnO powder as a sintering additive was found to be essential since high density ceramics could not be successfully produced without a sintering aid.

$Ba(Cd_{1/3}Ta_{2/3})O_3$ samples with 2 wt % ZnO additive were pressed at 60% of theoretical density and then sintered at 1450, 1520, 1550, and 1580 °C for 48 h in a Pt crucible with an initial ramp rate of 100 °C/h in air. During sintering, the crucible was sealed by Pt foil and the samples were covered with powder enhanced with additional CdO to reduce and offset the loss of this volatile component. The samples were slowly cooled and no additional postfiring heat treatments were used in this investigation.

Phase stability of powder was studied using a thermogravimetric measurement system (Setaram, TG_DTA92). In each run, the mass loss of powder was monitored at constant temperature ramp as a function of time. The powders were allowed to decompose to completion.

The structure of the powder and ceramics was characterized using a Rigaku D/MAX-IIB diffractometer. A single crystal graphite monochromator was used to attain Cu $K\alpha$ radiation. Polysilicon powder with a diameter of less than 75 μm was used as a reference standard. The lattice constants were determined by fitting at least 6 of the dominant diffraction peaks in the spectra using a least square error minimization fit in the MDI-Jade program with the pattern-indexing feature. Simulations of x-ray diffraction spectra were performed with the same software using the pattern calculation feature.

Immersion pycnometry was used to quantitatively determine the density for well-sintered samples. The bulk density of other samples was evaluated by measuring the dimensions and weight of the specimen.

The microwave quality factor Q, dielectric constant, and temperature coefficient of resonant frequency τ_f were measured with the $TE_{01\delta}$ mode of a dielectric resonator. The unloaded quality factor Q_0 was determined using techniques that are a variation on Ginzton.[15] Kajfez[16,17] has extended Ginzton's measuring and graphical techniques of using VSWR to measure Q_0 and coupling of the dielectric sample in a resonant cavity. The procedure consists of placing the cylindrical DR sample to be measured in a Au-coated aluminum cylindrical cavity of dimensions approximately three times greater than the measured sample. The $TE_{01\delta}$ mode is measured using S11 reflection data at the terminals of the one port cavity. S11 data is collected spanning the resonant frequency and the immediate lower and upper frequency bounds. This data is processed[16,17] using a fractional linear curve fitting routine and then graphically displayed as a Q circle on a Smith chart. Values of Q_0, loaded Q, and the coupling coefficient are also displayed, the routine using the over-determined system of equations derived from the S11 data. This method, which we will refer to as the dielectric resonator method, does not produce precise measurements of the dielectric constant (error $\sim \pm 20\%$) as a result of the near-field coupling between the dielectric resonator and the metal resonant cavity. However, it can give reasonable trends between materials when similar size dielectric samples are used. The temperature coefficient of resonant frequency was measured over a temperature range of 25–60 °C.

To accurately determine the dielectric constant ε_r, a different technique was used which utilizes an open sided, parallel plate holder. This concept, proposed originally by Hakki and Coleman, was further developed by Courtney, and has subsequently retained the name of the "Courtney method." In our measuring technique, we have adopted the additional refinements outlined by Wheless and Kajfez[18] that allow for the identification of the $TE_{01\delta}$ mode as well as other modes that arise in this measuring configuration. The DR sample of known dimensions is placed between the plates of the two ports Courtney holder and connected to a vector network analyzer in transmission mode. The coupling probes of the two ports are either magnetic loops or electric probes that can be oriented both horizontally and vertically. Using this flexibility of probe type and orientation, the resonant frequency of the desired $TE_{01\delta}$ mode to be measured can be isolated. Mode charts[18,19] are also of assistance in this mode identification process. Once the resonant frequency is identified, the transcendental formulations[20,21] are utilized and compared to provide the DR sample ε_r. Root finding and graphing routines in Mathematica[22] were used to extract the value for ε_r for each DR sample.

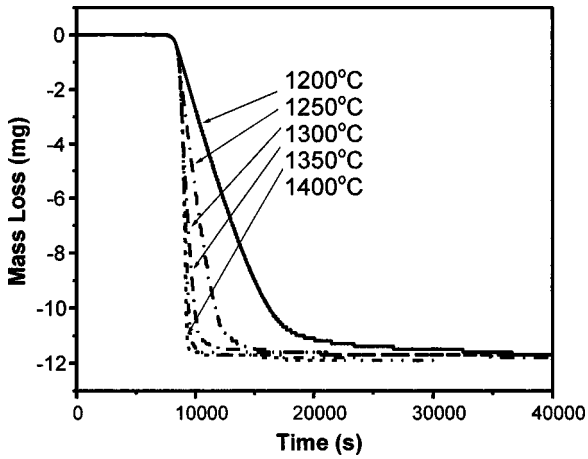

FIG. 1. Thermogravimetry measurements of the mass loss from $Ba(Cd_{1/3}Ta_{2/3})O_3$ as a function of time and temperature.

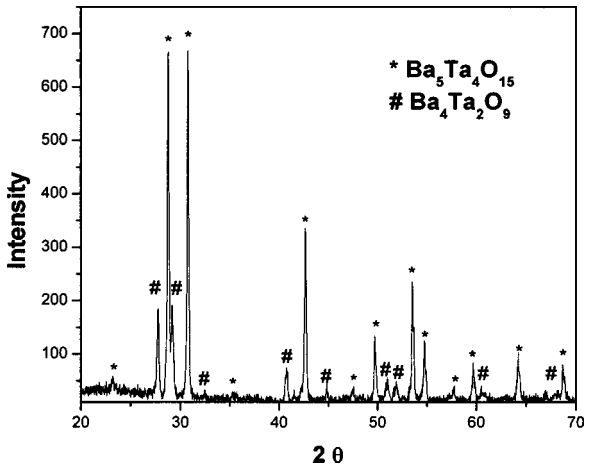

FIG. 2. X-ray diffraction spectra of decomposed $Ba(Cd_{1/3}Ta_{2/3})O_3$ powder after exposure to 1500 °C during the thermogravimetry measurements. Evidence of the presence of secondary $Ba_4Ta_2O_9$ and $Ba_5Ta_4O_{15}$ phases can be clearly seen.

Phonon frequencies and eigenmodes at the Γ point were calculated within the local-density approximation, using a full-potential, generalized linear muffin tin orbitals method.[23] Initially the lattice was relaxed assuming the $P\bar{3}m1$ symmetry associated with $Ba(Zn_{1/3}Ta_{2/3})O_3$. To compute phonon frequencies a frozen phonon approach was adopted by computing forces F_j for each of a sequence of small, finite displacement δx_i in coordinate i of the unit cell (there are three Cartesian components i for each site). The dynamical matrix was constructed by $V_{ij}=F_j/\delta x_i$ and the phonon eigenvalues determined from V_{ij}. Local orbitals[24] were used to include the Ba and Ta 5*p* states in the valence simultaneously with the usual 6*p* states. Local orbitals were found to be necessary for accurate total energies, as is often the case in transition-metal oxides with their short bond lengths. A rather large linear muffin-tin orbital basis set (about 15 orbitals/atom on average) was used, resulting in a well-converged local density approximation (LDA) calculation. It was found that for $Ba(Cd_{1/3}Ta_{2/3})O_3$ an imaginary phonon eigenvalue was found, indicating a symmetry-lowering distortion to P321 symmetry, bending the Ta–O–Cd bond from 180° as described below. The relaxation was traced until a zero-force condition was found. The Γ-point phonon eigenvalues were recalculated at the new positions and found to be positive, indicating a stable geometry.

III. RESULTS AND DISCUSSION

A. $Ba(Cd_{1/3}Ta_{2/3})O_3$ thermogravimetry experiments

Figure 1 shows thermogravimetry experiments that measure the mass loss of $Ba(Cd_{1/3}Ta_{2/3})O_3$ as a function of time and temperature. X-ray diffraction data of the resulting product, as shown in Fig. 2, indicate that $Ba(Cd_{1/3}Ta_{2/3})O_3$ decomposes according to the following reaction:

$$3Ba_3(CdTa_2)O_9(s) \rightarrow Ba_5Ta_4O_{15}(s) + Ba_4Ta_2O_9(s) + 3CdO(g).$$

The evaporation flux under equilibrium conditions is determined by the Hertz-Knudsen-Langmuir equation: $J_v=P_e(2\pi mkT)^{-1/2}$, where m is the molecular mass, k is the Boltzmman constant, and T is the temperature. Under conditions in which kinetic barriers are small, as would be expected for this system, the thermodynamic parameters for a thermally activated process can be deduced from $\Delta G=-RT\ln k$ and $\Delta G=\Delta H-\Delta ST$, where k is the reaction equilibrium constant and equals the partial pressure of CdO in this chemical reaction, and ΔG, ΔH, and ΔS correspond to Gibbs free energy, enthalpy, and entropy changes, respectively.

The evaporation rate, as inferred from the Hertz-Knudsen-Langmuir equation and the mass loss rate at maximum slope for each isothermal run, is plotted in Fig. 3. From this analysis, ΔH and ΔS of this decomposition reaction were determined to be 170.82 and 113.07 J/mol K, respectively. This plot represents a pressure-temperature phase diagram that is divided into two areas by the critical stability line. Above the line, $Ba(Cd_{1/3}Ta_{2/3})O_3$ is stable. Below the line, $Ba(Cd_{1/3}Ta_{2/3})O_3$ decomposes into $Ba_4Ta_2O_9$ and $Ba_5Ta_4O_{15}$. The results show that $Ba(Cd_{1/3}Ta_{2/3})O_3$ decomposes at a moderate rate at the temperature and pressures required for sintering.

B. X-ray diffraction

X-ray diffraction spectra of $Ba(Zn_xCd_{1/3-x}Ta_{2/3})O_3$ powders, as shown in Fig. 4, indicate that this system forms solid

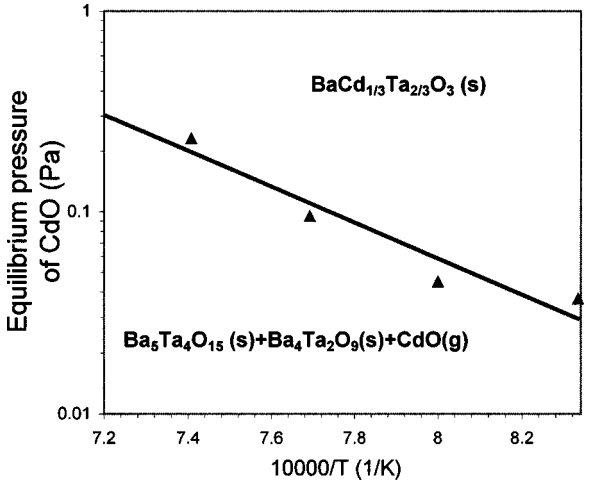

FIG. 3. Ellingham diagram for $Ba(Cd_{1/3}Ta_{2/3})O_3$.

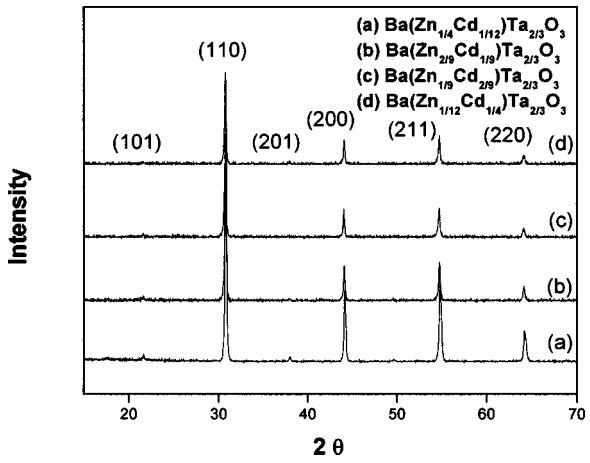

FIG. 4. X-ray diffraction spectra of $Ba(Cd_{1/3-x}Zn_xTa_{2/3})O_3$ solid solution powder.

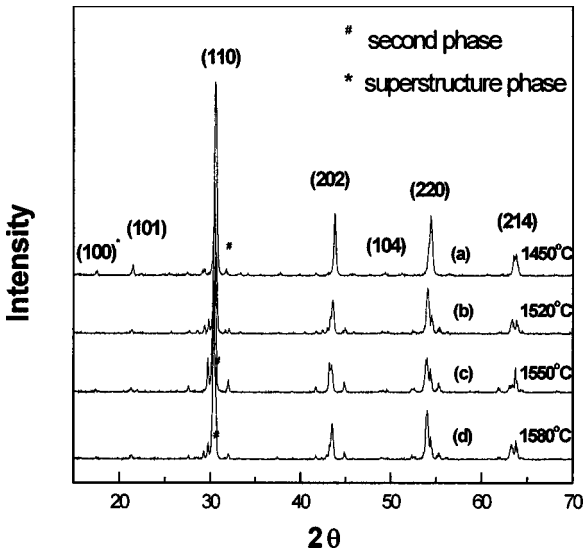

FIG. 5. X-ray diffraction spectra of sintered $Ba(Cd_{1/3}Ta_{2/3})O_3$ synthesized with 2 wt % ZnO as sintering aid.

solutions over the entire range of alloy compositions. The observed trend in the increase in lattice constant with increasing Cd content, summarized in Table I, is expected since the ionic radius of Zn^{2+} is smaller than that of Cd^{2+}. In this case, we labeled the x-ray diffraction (XRD) pattern in Fig. 4 using the notation of the cubic structure.

Figure 5 shows x-ray diffraction spectra of $Ba(Cd_{1/3}Ta_{2/3})O_3$ ceramics with 2 wt % ZnO as a sintering additive as a function of sintering temperature. Evidence for Cd–Ta ordering, as indicated by the presence of weak (100) superstructure peak in the x-ray diffraction spectra (indicated by an asterisk) near ~18° can been found. It should be noted that x-ray diffraction simulations of ordered structures indicate that the superstructure peak intensity of $Ba(Cd_{1/3}Ta_{2/3})O_3$ will be ~3 times smaller than that of $Ba(Zn_{1/3}Ta_{2/3})O_3$ for the same amount of ordering due to the smaller difference in scattering amplitude (i.e., smaller ΔZ) between Cd and Ta than between Zn and Ta. In our recently published work $Ba(Cd_{1/3}Ta_{2/3})O_3$ samples prepared with a boron oxide sintering aid found high intensity superlattice peaks using selected area electronic diffraction, although the XRD superlattice peaks were also very weak.[25] Earlier work by Jacobson[26] did not detect superlattice lines resulting from cation ordering for the Ba–Ta–Cd–O system.

Additional secondary phase XRD peaks in the Fig. 5 are found at the elevated temperature that does not match the expected decomposition product. They may be attributed to the formation of intermediate or metastable phases as a result of partial decomposition.

TABLE I. The lattice constants of $Ba(Zn_xCd_{1/3-x}Ta_{2/3})O_3$ powder samples fit to the cubic and hexagonal structure.

	a (Å) (cubic)	*a* (Å) (hexagonal)	*c* (Å) (hexagonal)
$Ba(Zn_{1/3}Ta_{2/3})O_3$	4.094	5.788	7.099
$Ba(Zn_{1/4}Cd_{1/12})Ta_{2/3}O_3$	4.104	5.802	7.109
$Ba(Zn_{2/9}Cd_{1/9})Ta_{2/3}O_3$	4.105	5.804	7.111
$Ba(Zn_{1/9}Cd_{2/9})Ta_{2/3}O_3$	4.146	5.868	7.193
$Ba(Zn_{1/12}Cd_{1/4})Ta_{2/3}O_3$	4.148	5.871	7.195
$Ba(Cd_{1/3}Ta_{2/3})O_3$	4.163	5.880	7.210

C. Density and microstructure

The density of $Ba(Cd_{1/3}Ta_{2/3})O_3$ is less than 80% when prepared without a sintering additive. Significantly improved densification is attained with the addition of ZnO as a sintering additive. Fig. 6 shows the dependence of sample density on sintering temperature. The small density of samples sintered above 1520 °C is presumably due to the evaporation of CdO, as would be expected from our thermogravimetry results.

Typical scanning electron microscopy of $Ba(Cd_{1/3}Ta_{2/3})O_3$ with 2 wt % ZnO after 1550 °C sintering for 48 h are shown in Fig. 7. There is significant grain growth compared with the starting powder (~1–2 μm).

D. Dielectric properties

Figure 8 illustrates the *Qf* product (i.e., microwave quality factor times resonant frequency) of $Ba(Cd_{1/3}Ta_{2/3})O_3$ samples sintered over a range of temperatures. It is clear that the *Qf* product of $Ba(Cd_{1/3}Ta_{2/3})O_3$ is improved substantially

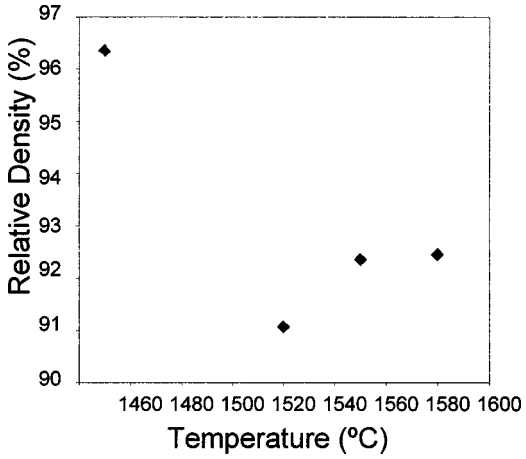

FIG. 6. Dependence of relative density on sintering temperature for $Ba(Cd_{1/3}Ta_{2/3})O_3$ ceramics synthesized with 2% ZnO sintering agent. Note: The theoretical density of $Ba(Cd_{1/3}Ta_{2/3})O_3$ is 7.94 g/cm^3.

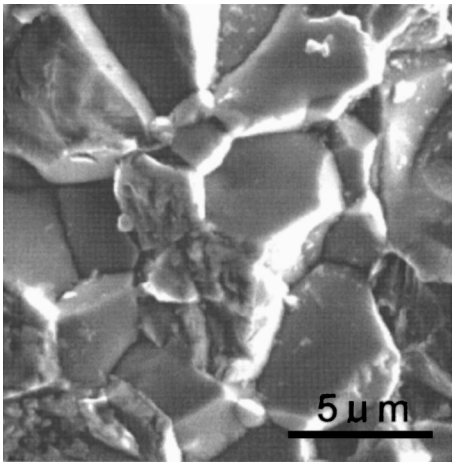

FIG. 7. Scanning electron micrograph of $Ba(Cd_{1/3}Ta_{2/3})O_3$ with 2 wt % ZnO sintered at 1550 °C for 48 h.

when a ZnO sintering agent is added. The Qf product exhibits a maximum at a sintering temperature of ~1550 °C. It is interesting to note that the highest Qf is attained in samples that contain a significant fraction of secondary phases. It is particularly surprising given that the decomposition products would not be expected to necessarily produce low-loss phases. The same phenomenon has been observed for $Ba(Zn_{1/3}Ta_{2/3})O_3$ when the loss of ZnO is correlated with a reduced microwave loss tangent.[27] The simultaneous appearance of ordering and secondary phases does not allow us to isolate the role of each of these parameters on the microwave dielectric properties using our current data.

Dielectric constants of $Ba(Cd_{1/3}Ta_{2/3})O_3$ with and without 2 wt % ZnO, as measured by the dielectric resonator method, are illustrated in Fig. 9. The Courtney method was used to verify the results in Fig. 9 determined from the following equation: $f=34/\sqrt{\varepsilon}a(a/t+3.54)$, where a is the sample radius in millimeters, t is the sample thickness in millimeters, ε is the relative dielectric constant, and f is the resonance frequency in gigahertz. The dielectric constant of $Ba(Cd_{1/3}Ta_{2/3})O_3$ doped with a 2 wt % ZnO sintering aid and sintered at 1550 °C measured with the Courtney method to

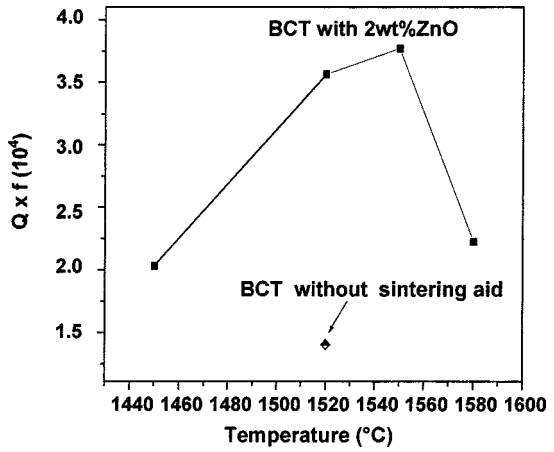

FIG. 8. Dependence of Qf on the sintering temperature of $Ba(Cd_{1/3}Ta_{2/3})O_3$ (BCT) samples synthesized with and without 2% ZnO sintering agent.

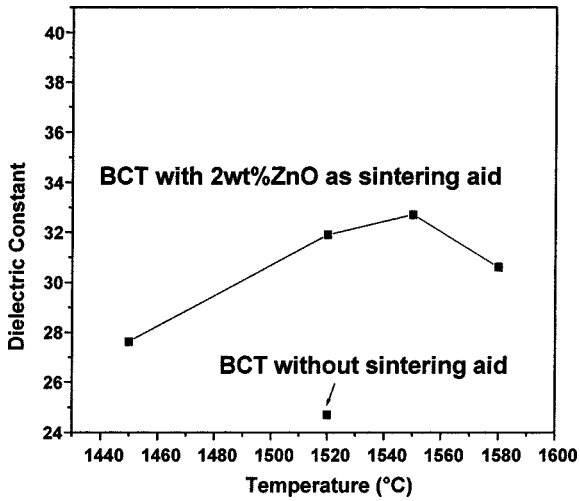

FIG. 9. Dependence of dielectric constant on sintering temperature for $Ba(Cd_{1/3}Ta_{2/3})O_3$ (BCT) samples synthesized with and without 2% ZnO sintering agent.

be ~32.5. This value is close to 33.2, the dielectric constant ε_r measured by the dielectric resonator method.

The temperature coefficient of resonant frequency τ_f is measured to be 80 ppm/°C for sample sintered at 1580 °C. The presence of a significant fraction of secondary phases does not allow us to confidently associate this value with the intrinsic parameter for this material. However, recent work by our group finds a similar value of 85±15 ppm/°C for $Ba(Cd_{1/3}Ta_{2/3})O_3$ prepared with a B_2O_3 sintering additive that has a significantly reduced fraction of secondary phases.[28]

E. Local density-functional calculation for $Ba(Cd_{1/3}Ta_{2/3})O_3$ and $Ba(Zn_{1/3}Ta_{2/3})O_3$

Ab initio calculations within the LDA of $Ba(Zn_{1/3}Ta_{2/3})O_3$ and $Ba(Cd_{1/3}Ta_{2/3})O_3$ predict equilibrium lattice constants of $a=0.574$, $c=0.700$ and $a=0.583$ nm, $c=0.717$ nm, respectively. The full-potential variant of the method of linear muffin tin orbitals employed[23] was described in Sec. II. Note that the c/a ratio is very near $(3/2)^{0.5}$, as is characteristic of an undistorted pseudocubic crystal. The predicted lattice constants are slightly smaller (0.01%–1%) than the experiment, as is typically found in the LDA. The $Ba(Cd_{1/3}Ta_{2/3})O_3$ bulk modulus was calculated to be 1.91 Mbar; slightly less than the value for $Ba(Zn_{1/3}Ta_{2/3})O_3$ (1.99 Mbar) as a result of the dilated lattice.

The most important difference between $Ba(Cd_{1/3}Ta_{2/3})O_3$ and $Ba(Zn_{1/3}Ta_{2/3})O_3$ is the additional distortion found in $Ba(Cd_{1/3}Ta_{2/3})O_3$ that results in a bond angle of 172° for the Ta–O–Cd bond. $Ba(Zn_{1/3}Ta_{2/3})O_3$ has a threefold rotation about the c axis, a twofold rotation about y, and finally an inversion symmetry, making 12 group operations in all. The relaxed positions for all atoms as calculated within the LDA are shown in Table II. The crystal structure for $Ba(Zn_{1/3}Ta_{2/3})O_3$ has a hexagonal Bravais lattice and is in the $P\bar{3}m1$ space group, see Fig. 10. The Bravais lattice for $Ba(Cd_{1/3}Ta_{2/3})O_3$ is also hexagonal, but a distortion of the O

TABLE II. Table of lattice positions in Cartesian coordinates. Note: The dimensions are scaled to the cubic unit cell dimensions.

	BZT			BCT		
Ba2	0.0000	0.0000	0.0000	0.0000	0.0000	0.0000
Ba	0.3333	−0.3333	0.3386	0.3333	−0.3333	0.3398
Ba	−0.3333	0.3333	−0.3386	−0.3333	0.3333	−0.3398
Ta	0.3333	−0.3333	−0.1754	0.3333	−0.3333	−0.1670
Ta	−0.3333	0.3333	0.1754	−0.3333	0.3333	0.1670
Zn(Cd)	0.0000	0.0000	−0.5000	0.0000	0.0000	0.5000
O1	0.0000	−0.5000	0.0000	0.0000	−0.4836	0.0000
O1	−1.5000	−0.5000	0.0000	0.4836	0.4836	0.0000
O1	0.5000	0.0000	0.0000	−0.4836	0.0000	0.0000
O2	0.1714	0.3428	−0.3245	0.1539	0.3507	−0.3153
O2	−0.1714	−0.3428	0.3245	−0.1969	−0.3507	0.3153
O2	−0.1714	0.1714	0.3245	−0.1539	0.1969	0.3153
O2	0.3428	0.1714	0.3245	0.3507	0.1539	0.3153
O2	−0.3428	−0.1714	−0.3245	−0.3507	−0.1969	−0.3153
O2	0.1714	−0.1714	−0.3245	0.1969	−0.1539	−0.3153

atoms between Ta and Cd lowers the energy and breaks the inversion symmetry as discussed in Sec. II. Unfortunately it is not possible to detect experimentally whether this distortion actually exists, because the intensity difference of the simulated x-ray spectra resulting from the distortion of the oxygen atoms is only 0.01%. This change is too small to be distinguished experimentally since other factors including the presence of strain and varying degrees of order in the *B*-site sublattice can result in similar modifications to the spectra.

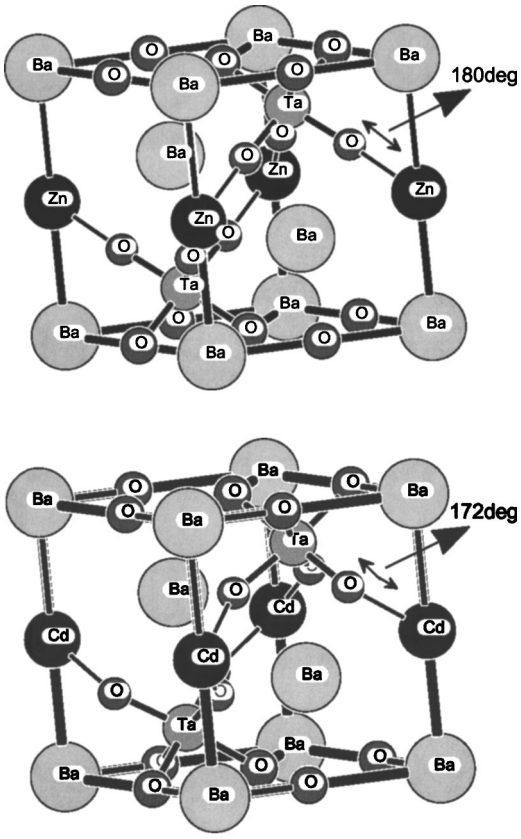

FIG. 10. Ball and stick model of (a) $Ba(Zn_{1/3}Ta_{2/3})O_3$ and (b) $Ba(Cd_{1/3}Ta_{2/3})O_3$. Solid black balls are Zn in (a) and Cd in (b). The distortion relative to the bond-centered configuration has been amplified by a factor of 5 to more clearly show the distortion, in particular, the buckling of the Ta–O–Cd bond.

The energy of the crystal as a function of the oxygen distortion is illustrated in Fig. 11, with the minimum in energy representing the relaxed position shown in Table II. Note that the oxygen atom would be expected to oscillate between these positions at room temperature since the energy barrier separating the minima (6 meV) is small compared to thermal energies (26 meV). Interestingly, even though $Ba(Cd_{1/3}Ta_{2/3})O_3$ was found to have this distortion while $Ba(Zn_{1/3}Ta_{2/3})O_3$ did not, the phonon modes were found to be fairly similar, with the Cd-bearing case having slightly softer modes at lower energy and stiffer modes at high energy. Nevertheless the phonon mode associated with the O distortion would be anticipated to have a strong anharmonic component in the Cd-bearing case.

It is interesting that both $Ba(Zn_{1/3}Ta_{2/3})O_3$ and $Ba(Cd_{1/3}Ta_{2/3})O_3$ are expected to have atypical physical properties due to its unusual *d*-electron bonding. The presence of significant charge transfer between the cation *d*-orbitals is predicted to provide a degree of covalent directional bonding between atoms that resist angular distortions,

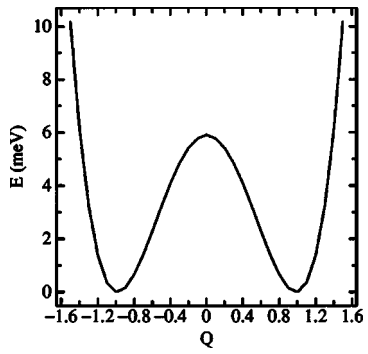

FIG. 11. Energy as a function of the generalized coordinate *Q*. *Q* parametrizes the collective displacement of the O atoms; $Z=0$ corresponds to the high-symmetry position of the oxygen atom between the Cd and Ta atoms; $Q=1$ to the minimum energy configuration given in Table II.

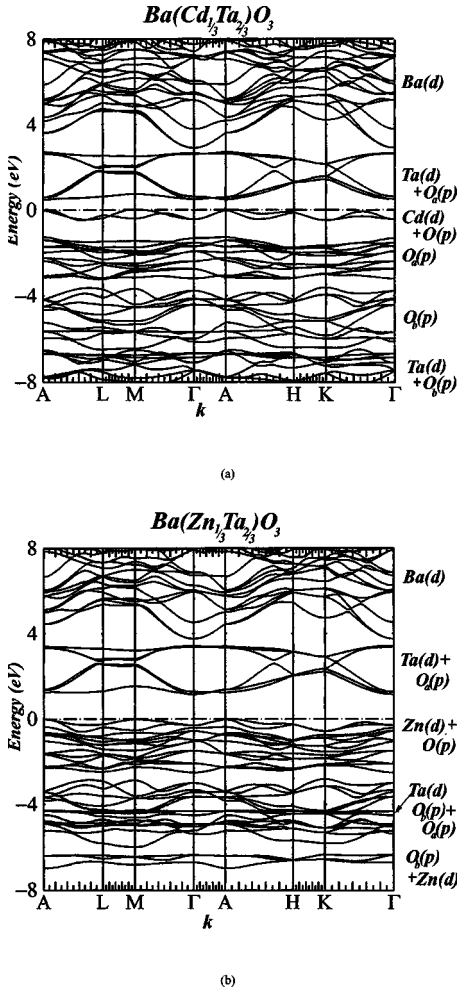

FIG. 12. Electronic band structure of (a) $Ba(Cd_{1/3}Ta_{2/3})O_3$ and (b) $Ba(Zn_{1/3}Ta_{2/3})O_3$ as calculated by the linear muffin tin orbital method within the local density functional approximation.

a property absent in conventional ionic compounds. This may strengthen "soft lattice modes" correlated with microwave loss, as might occur in both defective and high-quality ionic compounds. The influence of the *d*-electron type bonding, as compared to conventional nondirectional metal-oxygen ionic bonding, may play an important role in achieving high melt temperatures and enhanced phonon energies. The latter may presumably play a role in the ultralow microwave loss (loss tangent) that is observed in this class of materials. In the case of $Ba(Cd_{1/3}Ta_{2/3})O_3$ and $Ba(Zn_{1/3}Ta_{2/3})O_3$, our theoretical work using the LDA approximation indicates that charge is transferred from Ta 5*d* levels in the conduction band (empty states near the conduction band minimum) to Cd-4*d* and Zn-3*d* levels (full states near the valence band maximum), see Fig. 12. Typically phonon energies scale inversely with the bond distance. Therefore, high *Z* materials tend to have reduced phonon energies and enhanced loss tangents. The high dielectric constant of high *Z* material is a result of the large polarizability of the core electrons. We speculate that the presence of a significant amount of *d*-electron covalent bonding in a compound with many high-*Z* components such as $Ba(Cd_xZn_{1/3-x}Ta_{2/3})O_3$ can result in enhanced the phonon energies, possibly resulting in reduced microwave loss, while still maintaining a large dielectric constant.

IV. CONCLUSION

While $Ba(Zn_xCd_{1/3-x}Ta_{2/3})O_3$ alloy ceramics with high densities could not be attained without the aid of a sintering agent, the addition of 2 wt % ZnO was needed to achieve over 97% of the theoretical density for pure $Ba(Cd_{1/3}Ta_{2/3})O_3$ ceramics. Evidence for Cd–Ta ordering, as indicated by the presence of superstructure peaks in the x-ray diffraction spectra, was found. For a sample sintered at 1550 °C for 48 h, the dielectric constant and microwave loss tangent were measured to be ~ 32 and 5×10^{-5} at 2 GHz. Local density functional calculations of $Ba(Cd_{1/3}Ta_{2/3})O_3$ and $Ba(Zn_{1/3}Ta_{2/3})O_3$ give insight into the unusual nature of this class of material. The conduction band maximum and valence band minimum are strongly composed of weakly itinerant Ta 5*d*-and Zn-3*d*/Cd-4*d* levels, respectively. This is believed to play an important role in having a high melt temperature and enhanced phonon energies, as well as the unusual property of having both a high dielectric constant and low loss tangent.

ACKNOWLEDGMENTS

The authors wish to thank Timothy W. Karcher for assistance in thermogravimetric measurements and Dr. William Petuskey, David Wright, and Tom Groy for their advice throughout the project. The Office of Naval Research under Contract No. N000140010550 and the ASU Wintech Center provided support for this work.

[1] K. Wakino, T. Nishikawa, Y. Ishikawa, and H. Tamura, Br. Ceram. Trans. J. **89**, 39 (1990).
[2] D. Davies, Ceram. Trans. **53**, 137 (1995).
[3] G. Rong, N. Newman, B. Shaw, and D. Cronin, J. Mater. Res. **14**, 4011 (1999).
[4] J. Pond, S. Liu, and N. Newman, IEEE Trans. MTT 49, 2363 (2001).
[5] T. Negas, G. Yeager, S. Bell, and R. Amren, *Chemistry of Electronic Ceramic Materials*, Proceedings of the international conference, Jackson, Wyoming, 17–20 July, 1990 (National Institute of Standards and Technology Special Publications, Gaithersburg, MD, 1991), p. 21.
[6] H. Tamura, T. Konoike, Y. Sakabe, and K. Wakino, J. Am. Ceram. Soc. **67**, C59 (1984).
[7] R. Zurmühlen *et al.*, J. Appl. Phys. **77**, 5351 (1995).
[8] D. A. Sagala and S. Nambu, J. Phys. Soc. Jpn. **61**, 1791 (1992).
[9] S. Kamba *et al.*, J. Phys. D **37**, 1980 (2004).
[10] D. Sagala and S. Nambu, J. Am. Ceram. Soc. **75**, 2573 (1992).
[11] Y. Park and Y. Kim, Mater. Res. Bull. **31**, 7 (1996).
[12] P. Davies, J. Tong, and T. Negas, J. Am. Ceram. Soc. **80**, 1727 (1997).
[13] V. Tolmer and G. Desgardin, J. Am. Ceram. Soc. **75**, 2573 (1992).
[14] A. K. Ganguii, K. P. Jayadevan, G. N. Subbanna, and K. B. R. Varma, Solid State Commun. **94**, 13 (1995).
[15] E. L. Ginzton, Microwave Measurements (McGraw-Hill, New York, 1957).
[16] D. Kajfez, *Q Factor, Vector Fields* (Oxford, MS, 1994).
[17] D. Kajfez, IEEE Trans. MTT 42, 1149 (1994).
[18] P. Wheless and D. Kajfez, IEEE MTT-S Symposium Dig. 473 (1985).
[19] W. E. Courtney, IEEE Trans. MTT 18, 476 (1970).
[20] B. W. Hakki and P. D. Coleman, IEEE Trans. MTT 8, 402 (1960).
[21] C. C. Johnson, *Field and Wave Electrodynamics* (McGraw-Hill, New York, 1965), pp. 173–176.
[22] S. Wolfram, The Mathematica book, 4th ed. (Wolfram Media / Cambridge University Press, Champaign, IL / Melbourne, Australia, 1999).
[23] M. Methfessel, M. van Schilfgaarde, and R. A. Casali, in *Electronic Structure and Physical Properties of -Solids: The Uses of the LMTO Method*, Lecture Notes in Physics, edited by H. Dreysseed (Springer, Berlin, 2000), Vol. 535.

[24]D. Singh, Phys. Rev. B **43**, 6388 (1991).
[25]J. Sun, S. Liu, N. Newman, and D. J. Smith, Appl. Phys. Lett. **84**, 3918 (2004).
[26]J. Jacobson, B. M. Collins, and B. E. F. Fender, Acta Crystallogr., Sect. B: Struct. Crystallogr. Cryst. Chem. **B32**, 1083 (1976).
[27]S. B. Desu and H. M. O'Bryan, J. Am. Ceram. Soc. **68**, 546 (1985).
[28]S. Liu, J. Sun, R. Taylor, D. J. Smith, and N. Newman, J. Mater. Res. **19**, 3526 (2004).